tvst

Article

Anatomical Location of the Raphe and Extended Raphe in the Human Retina: Implications for Assessment of the Optic Nerve with OCT

Nomdo M. Jansonius[1,2] and Ulrich Schiefer[3,4]

[1] Department of Ophthalmology, University Medical Center Groningen, University of Groningen, Groningen, The Netherlands
[2] Graduate School of Medical Sciences, Research School of Behavioural and Cognitive Neurosciences, University of Groningen, Groningen, The Netherlands
[3] Study Course Ophthalmic Optics, Aalen University of Applied Sciences, Aalen, Germany
[4] Centre for Ophthalmology, University of Tübingen, Tübingen, Germany

Correspondence: N.M. Jansonius, Department of Ophthalmology, University Medical Center Groningen, University of Groningen, P.O. Box 30.001, 9700 RB Groningen, The Netherlands. e-mail: ulrich.schiefer@hs-aalen.de, n.m.jansonius@umcg.nl

Received: February 2, 2020
Accepted: September 1, 2020
Published: October 6, 2020

Keywords: optical coherence tomography; retinal nerve fiber layer; retinal nerve fiber bundle trajectories; structure function; glaucoma

Citation: Jansonius NM, Schiefer U. Anatomical location of the raphe and extended raphe in the human retina: Implications for assessment of the optic nerve with OCT. Trans Vis Sci Tech. 2020;9(11):3, https://doi.org/10.1167/tvst.9.11.3

Purpose: To determine the location of (1) the superior–inferior watershed between the fovea and optic disc (extended raphe) at the peripapillary optical coherence tomography (OCT) measurement circle and (2) the raphe, temporal to the fovea.

Methods: We used existing data consisting of 2285 traced retinal nerve fiber bundle trajectories from 83 fundus images. For localization of the extended raphe at the 3.46-mm-diameter OCT measurement circle, trajectories were classified as belonging to the superior or inferior hemiretina, using predefined criteria. For the raphe, we localized the endings of trajectories coming from the superior and inferior arcuate bundles.

Results: At the measurement circle, the extended raphe is located 14° (range, 12°–16°) inferiorly to a horizontal line through the optic disc center. The raphe follows a horizontal line at the latitude of the fovea if the disc is assumed to be located 15° nasal to and 2° above the fovea.

Conclusions: At the measurement circle, OCT brands use either the 9 o'clock location or a straight line connecting the center of the optic disc and the fovea as a reference for separating the hemiretinas. This results, on average, in a 14° and 6° misalignment with respect to the anatomical watershed, respectively. For the macular area, the commonly used line through the center of the optic disc and the fovea fails to describe the raphe adequately.

Translational Relevance: An unbiased asymmetry assessment of the optic nerve requires a detailed knowledge of the shape and location of the (extended) raphe.

Introduction

Superior–inferior asymmetry is a hallmark of many optic neuropathies, including glaucoma and ischemic optic neuropathy. An unbiased assessment of this asymmetry requires a detailed knowledge of the anatomy of the retinal nerve fiber bundle (RNFB) trajectories and, especially, the location of the raphe, which is located temporal to the fovea, and the superior–inferior watershed between the fovea and optic disc, referred to here as the extended raphe. The (extended) raphe is the seam where the nerve fiber bundles of the superior and inferior hemiretina meet each other, functionally resulting in a nasal step or altitudinal visual field defect. Knowledge regarding the exact location of the raphe and extended raphe, and the variability therein, is incomplete. Added to that, the implementation of this knowledge in current, commercially available optical coherence tomography (OCT) devices seems rather crude and imprecise.

There are two regions of interest for the assessment of optic nerve pathology with OCT: the optic disc region and the macular region. In the optic disc region, the focus is on the peripapillary retinal nerve fiber layer (pRNFL) thickness; in the macular region, the focus is on the thickness of the inner retinal layers. The pRNFL thickness is measured at a circle with a diameter of 3.46 mm around the center of the optic disc.[1–3] On this measurement circle, OCT brands use either the 9 o'clock location (e.g., Canon) or the intersection with a line through the center of the optic disc and the fovea (e.g., Heidelberg Engineering) as a reference for separating the hemiretinas. For the macular region, most OCT brands use a line through the center of the optic disc and the fovea to separate the hemiretinas.

We developed a modified polar coordinate system for the human retina, originally used as a reference for our RNFB trajectory model.[4] Coordinate systems are, in principle, arbitrary, and we can always swap between systems by using transformations; however, a well-chosen system facilitates mathematics and interpretation. In the modified polar coordinate system, one of the major axes was chosen to coincide with the separation between the superior and inferior hemiretina. In the current study, we validate this coincidence. The concerning axis, referred to here as the modified polar coordinate system reference line, is not a straight line but rather a combination of a straight section temporal to the fovea and a curved section (parabola with horizontal tangent in the fovea) between the fovea and the center of the optic disc. "Horizontal" was defined as parallel to the straight section temporal to the fovea; this orientation was imposed on an assumed position of the center of the optic disc relative to the fovea. As such, the system is invariant of head tilt or eye rotation during image acquisition (see Discussion section). The position of the center of the optic disc relative to the fovea was inspired by perimetry. Two observations from perimetry contributed here: (1) arcuate scotomata (nasal steps) rarely cross the horizontal meridian within the accuracy of the applied testing grids, which test up to 1° (10-2) or 3° (24-2 and 30-2) from the horizontal meridian, and (2) the center of the blind spot is located on average 2° below the horizontal meridian and 15° temporal to fixation.[5–7] Figure 1 shows the modified polar coordinate system reference line together with the 3.46-mm-diameter peripapillary OCT measurement circle and the various OCT reference lines.

The aim of this study was to determine the location of (1) the extended raphe at the peripapillary OCT measurement circle and (2) the raphe. For this purpose, we used previously collected datasets consisting of a large number of traced RNFB trajectories from high-quality red-free fundus images.[4,8] For the localization of the extended raphe at the measurement circle, the trajectories in the papillomacular bundle were classified (using predefined criteria) as belonging to the superior or inferior hemiretina. For the localization of the raphe, we used the coordinates of the endings of the trajectories coming from the superior and inferior arcuate bundles. For both locations, the results were compared to the modified polar coordinate system reference line and the reference lines currently used in commercially available OCT devices.

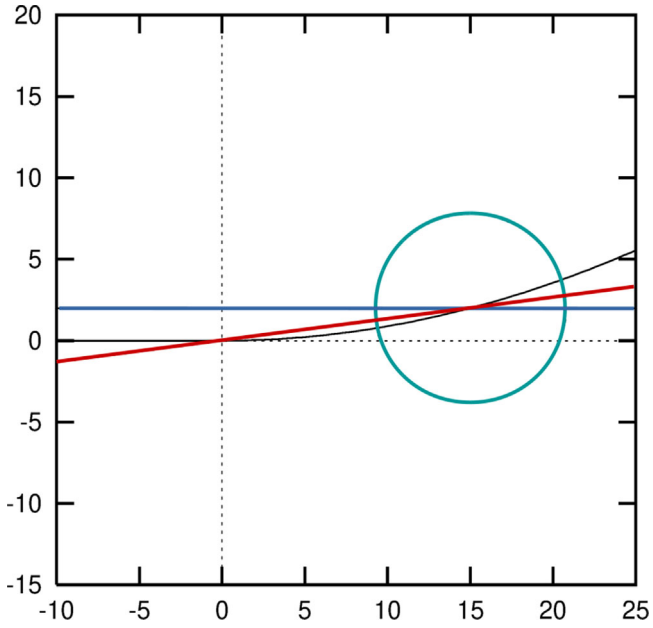

Figure 1. Reference lines used in the current study plotted in a Cartesian coordinate system that has its origin at the fovea. Axes are in degrees. The *black line* is the modified polar coordinate system reference line. It is a combination of a straight section temporal to the fovea and a curved section (parabola with horizontal tangent in the fovea) between the fovea and the center of the optic disc, which is, by definition of the modified polar coordinate system,[4] located at (15,2) in the Cartesian coordinate system. The *turquoise circle* represents the 3.46-mm-diameter OCT measurement circle. The *blue line* represents a horizontal line through center of optic disc; locations at the OCT measurement circle are depicted in degrees relative to this line. Hence, the *blue line* crosses the circle at 0° (nasal) and 180° (temporal). The *red line* goes through the center of the optic disc and the fovea. It crosses the OCT measurement circle at 188°. The *black line* crosses the measurement circle at 193°.

Methods

Study Population and Data Collection

We used two previously collected datasets, each consisting of a large number of traced retinal nerve fiber bundle trajectories from high-quality red-free

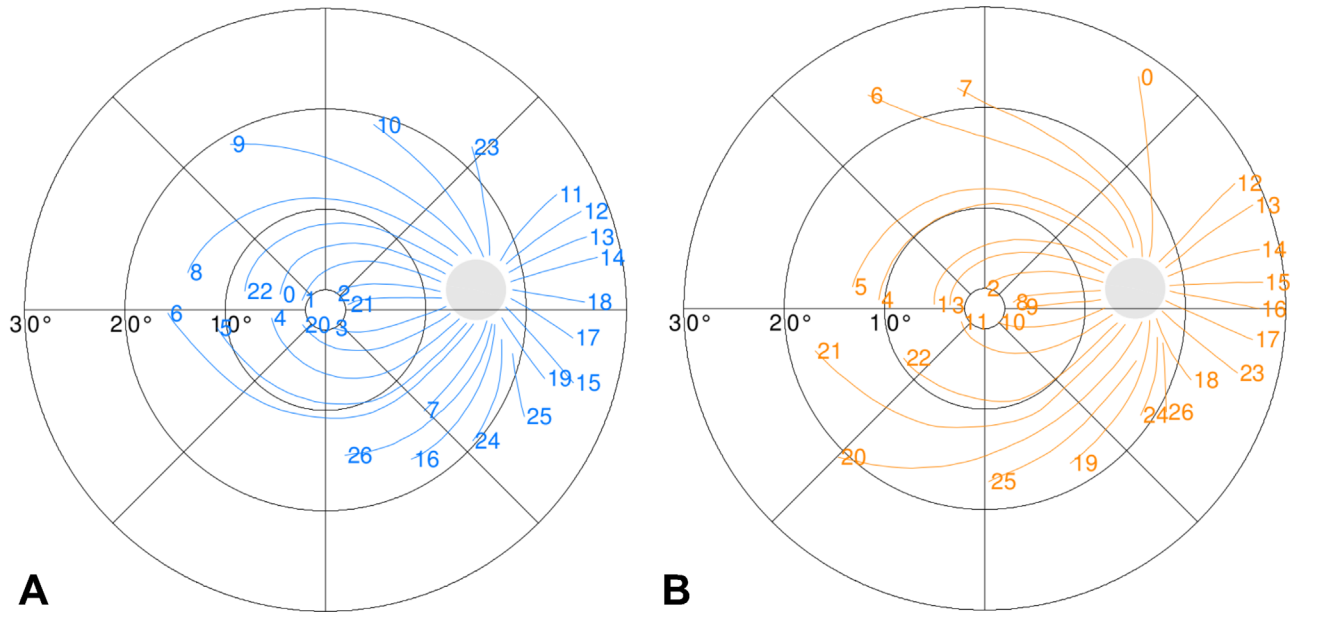

Figure 2. Examples of trajectory classifications in the papillomacular bundle. (**A**) Subject with the trajectories classified as superior (trajectories 2 and 21) and inferior (trajectory 3). (**B**) Subject with the trajectories classified as superior (8), equivocal (9), and inferior (10).

fundus images.[4,8] The first dataset used in the current study was comprised of 28 fundus pictures of the right eyes of 28 subjects.[8] The pictures were selected from patients who underwent digitized fundus photography as part of regular ophthalmic care in the University Eye Hospital Oulu, Finland. To ensure good visibility, only subjects without diseases affecting the RNFL or its visibility were included (mostly diabetic patients without diabetic retinopathy). Mean refraction was -0.4 ± 3.3 diopters (D). Supplementary Figure S1 shows the papillomacular region of all 28 subjects. In this dataset, we systematically traced one trajectory of a predefined minimum length in each half clock-hour to obtain a complete picture of the RNFB trajectory pattern. Approval for the data collection was obtained according to the guidelines of the Ethical Committee of the Northern Ostrobothnia Hospital District. All subjects provided written informed consent. The study followed the tenets of the Declaration of Helsinki. The second dataset was comprised of 55 fundus pictures of 55 subjects from our original study.[4] Neither refraction nor axial length was recorded in this dataset. On average, 30 trajectories per picture (range, 3–118) were traced, of various lengths and at various locations.

Data Analysis

Location of the Extended Raphe at the Peripapillary OCT Measurement Circle

For this analysis, we only used the first dataset, because in this dataset we had a complete, unbiased trajectory sampling in each half clock-hour. The trajectories were plotted for each subject separately (Fig. 2). We identified, for each subject, three trajectories in the papillomacular (PM) bundle. Subsequently, we classified these trajectories as belonging to either the superior hemifield or the inferior hemifield or as equivocal. For the trajectory to be classified as belonging to the superior hemifield, we required that it be convex toward the superior hemifield, or straight AND to end above a horizontal line through the fovea ($y > 0$ in Cartesian coordinates). For the trajectory to be classified as belonging to the inferior hemifield, it had to be convex toward the inferior hemifield, or straight AND had to end below a horizontal line through the fovea ($y < 0$ in Cartesian coordinates). If a trajectory within the PM bundle did not fulfill the criteria for either superior or inferior, it was classified as equivocal. The examples shown in Figure 2 belong to subjects with the trajectories classified as superior and inferior (Fig. 2A) and as superior, equivocal, and inferior (Fig. 2B), respectively. Finally, we recorded the location of the trajectories at the OCT measurement circle (Fig. 1), and we compared the resulting distributions for the superior, inferior, and equivocal trajectories. Locations at the measurement circle are expressed in degrees relative to the blue line in Figure 1, with 180° and 0° being the 9 o'clock and 3 o'clock locations, respectively, in the right eye.

Location of the Raphe

For this analysis, we used both datasets. For each dataset, we plotted all traced trajectories in a single

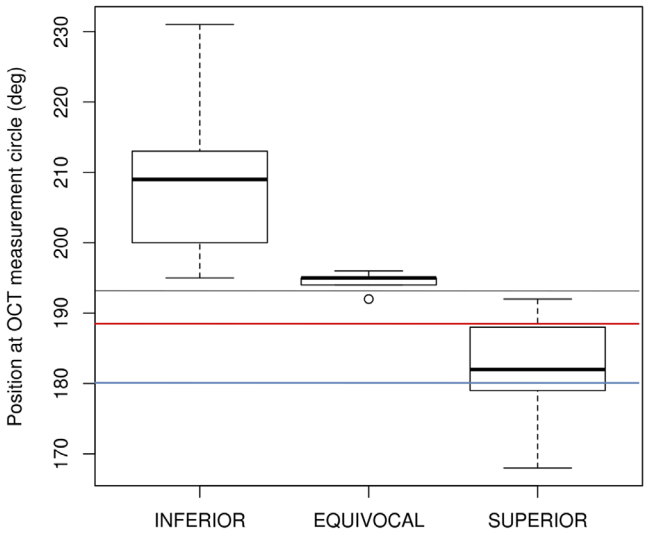

Figure 3. Distributions of the locations of the trajectories at the OCT measurement circle for trajectories classified as inferior, equivocal, or superior. Boxplots show median, interquartile range, minimum, and maximum; the circle represents an outlier. The *blue*, *red*, and *black lines* in Figure 1 cross the measurement circle at 180°, 188°, and 193°, respectively.

plot. The location of the raphe was defined as the middle of the trajectory-free zone temporal to the fovea.

Results

Location of the Extended Raphe at the Peripapillary OCT Measurement Circle

Figure 3 presents the distributions of the locations of the trajectories at the OCT measurement circle for (from left to right) trajectories classified as inferior, equivocal, and superior. Trajectories classified as superior and inferior did not show any overlap (maximum superior 192°, minimum inferior 195°); trajectories classified as equivocal ranged from 192° to 196°. Hence, a reasonable estimate of the location of the extended raphe at the OCT measurement circle is 194° ± 2°. This value deviates 14° from the crossing of the circle with a horizontal line through the center of the optic disc (blue line in Fig. 1) and 6° from the crossing of the circle with a line through the center of the optic disc and the fovea (red line in Fig. 1). Interestingly, the crossing of the extended raphe with the circle coincides almost perfectly with that of the modified polar coordinate system reference line (black line in Fig. 1), which crosses the circle at 193°.

Location of the Raphe

Figure 4 reveals the location of the raphe for both datasets. For the first dataset (Fig. 4A), one trajectory from the superior hemifield crossed the *x*-axis and two trajectories from the superior hemifield touched the *x*-axis; none of the trajectories from the inferior hemifield crossed or touched the *x*-axis. For the second dataset (Fig. 4B), some trajectories from the inferior hemifield crossed or touched the *x*-axis, whereas only one trajectory from the superior hemifield touched the *x*-axis. As such, taking both datasets into consideration, the location of the raphe appears to coincide essentially with the *x*-axis of the Cartesian coordinate system, which equals the modified polar coordinate system reference line (black line in Fig. 1) temporal to the fovea.

Discussion

At the 3.46-mm-diameter peripapillary OCT measurement circle, the extended raphe is located 14° ± 2° inferiorly to a horizontal line through the center of the optic disc. The raphe follows a horizontal line at the latitude of the fovea if the optic disc is assumed to be located 15° nasal to and 2° above the fovea.

The location of the raphe has been reported before as the disc–fovea–raphe angle. Using an adaptive-optics scanning laser ophthalmoscope, Huang et al.[9] reported this angle to be 170.3° ± 3.6°. Using OCT, Tanabe et al.[10] found 169° ± 3° and Bedggood et al.[11–13] found 173° ± 3°. With a disc–fovea angle of 7.6° (see next paragraph), our reference line (black line in Fig. 1) implies a disc–fovea–raphe angle of 180 – 7.6 = 172.4°. Hence, our findings are in good agreement with the literature. The disc–fovea–raphe angle was reported not to depend on the axial length.[10,12] This agrees well with our findings, as we found an equivocal location of the raphe (Fig. 4) despite a wide axial length range.

The location of the optic disc relative to the equator (optic disc inclination or fovea–disc angle (i.e., the angle between the Cartesian *x*-axis and the red line in Fig. 1)) was assumed to be 7.6° (arctan[2/15]) in our model. Earlier studies reported a mean value between 5° and 10° with a standard deviation of typically 3°.[6,8,10,12,14–18] Part of the observed variability will be real variability (i.e., related to individual retinal morphology); head tilt or eye rotation during image acquisition could have contributed, as well. Similarly, the distance between the fovea and the optic disc shows inter-individual variability, both when measured

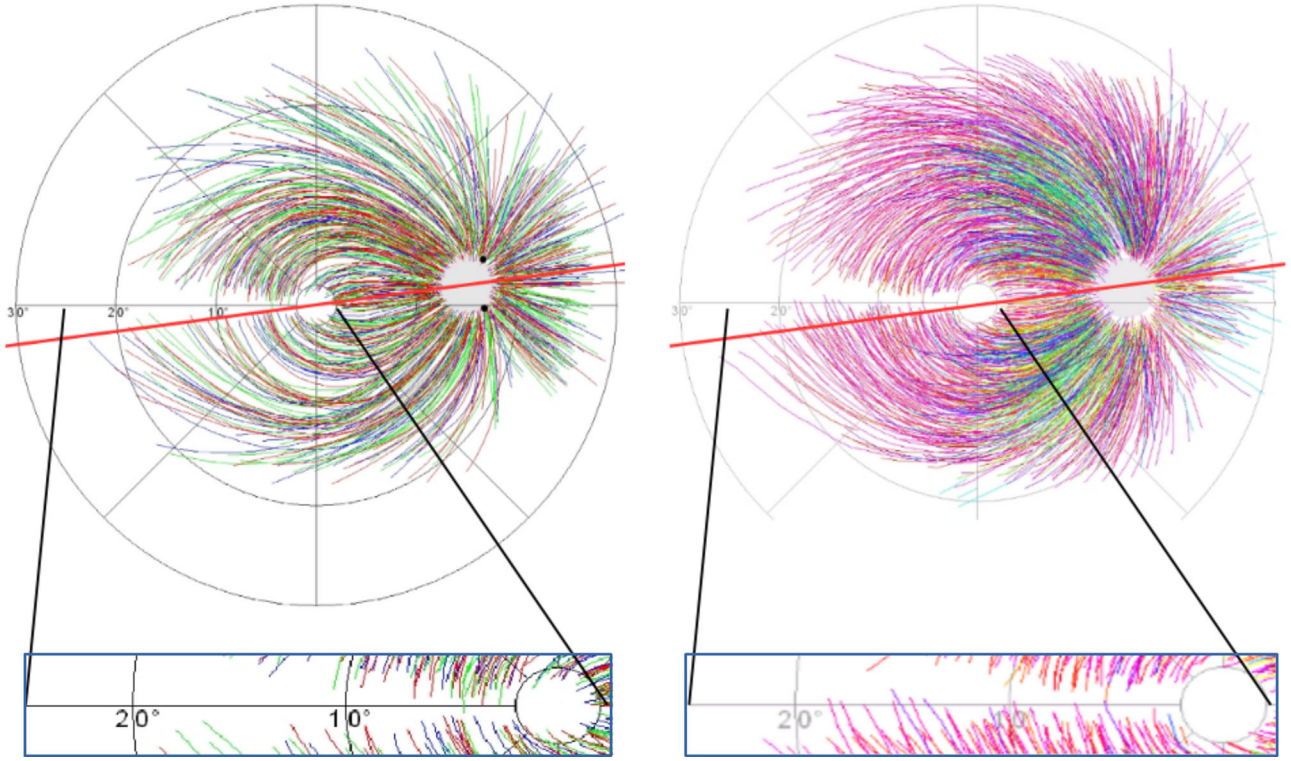

Figure 4. Superposition of all traced trajectories from the first (**A**) and second (**B**) datasets. Inserts show a magnified view of the area temporal to the fovea. The *red line* connects the center of the optic disc and the fovea.

in degrees[6] and when measured in millimeters.[16,18] By using the modified polar coordinate system, we assumed a uniform location of the optic disc relative to the fovea, thus entangling the above-mentioned sources of variability. Despite this assumption, we found, interestingly, very little variability in the location of the extended raphe at the peripapillary OCT measurement circle (Fig. 3) and the raphe (Fig. 4). This implies that a significant part of the variability of the optic disc inclination as reported in the literature actually is variability due to head tilt or eye rotation during image acquisition and paves the way for a simple and robust implementation of a less biased location of the (extended) raphe in OCT analysis software (see below). The variability reducing effect of our alignment procedure has been verified independently (figure 15 in Reference 19).

A limitation of our study is that only one of the datasets, with sample size $n = 28$, allowed for determination of the location of the intersection of the extended raphe and the peripapillary OCT measurement circle. However, the dataset covered a wide axial length range (20.4–26.2 mm; spherical equivalent from –8.75 to +6.25 D),[8] and, despite the wide axial length range, the location of the equivocal trajectories at the measurement circle had a very small range (192°–196°). Obviously, larger datasets would contain more extreme values either because of an increased likelihood of including rare anatomical variants or simply due to increased scattering with increased sample size.[20] Nevertheless, given the small range in our dataset, it is very unlikely that the mean of a much larger dataset would be closer to the red or blue line in Figure 1 (which intersect the measurement circle at 188° and 180°, respectively) than to the black line, our presumed extended raphe (which intersects the measurement circle at 193°).

Our dataset was limited to Caucasian eyes and did not explicitly address high myopia. Recently, we validated our trajectory model in Chinese eyes and specifically addressed high myopia (spherical equivalent beyond –6.00 D). Up to moderate myopia, the trajectories of the Chinese eyes were very similar to that of the Caucasian eyes. The high-myopic Chinese eyes deviated in the inferior–temporal region but not in the superior–temporal region.[17] In none of our analyses did we consider age as a covariate due to sample size limitations. A strength of our study is that the location of the raphe was replicated in an independent dataset.[4] Another strength is the fact that the trajectories were traced before the images were put in the modified polar coordinate system. As such, those who traced the trajectories were blinded with respect to the assumed

position of the watershed, and, even more, they were not aware of the purpose of the current analysis. It has been reported that manual tracing shows significant variability.[21] The authors of that study quantified variability as an uncertainty in the insertion point (angle) at the optic disc border. In our experience, the part closest to the optic disc is the most difficult part to trace; many trajectories could not be followed up to the optic disc at all. For that reason, we focused on the OCT measurement circle, where the uncertainty is much smaller.

Sugita et al.[22] automatically traced retinal nerve fiber bundle trajectories using polarization-sensitive OCT. Their region of interest (ROI) included the optic disc region and the papillomacular bundle. Their data, collected in four eyes of two subjects, support the nonlinear shape of the extended raphe. Obviously, their sample size is too small to draw conclusions regarding the anatomy of the human retina; their aim was to show the feasibility of automated tracing. They did not address the raphe. Although automated tracing has many advantages, the underlying techniques also have black box properties, and as such, manual tracing (once surpassed by automated techniques) still has its value for validating the automated techniques. Finally, the observed endings of the RNFB trajectories are not necessarily the real endings, and after the ending of a bundle the individual axons will continue their way to the retinal ganglion cell bodies. All of this introduces some uncertainty regarding the exact location of the watershed; however, there is no reason to assume that this uncertainty systematically biases the location of the raphe toward either superiorly or inferiorly. Finally, it should be mentioned that it is the superficially located RNFBs that have primarily been traced, as the more deeply located bundles are invisible on fundus images.

At the 3.46-mm-diameter peripapillary measurement circle, OCT brands use either the 9 o'clock location or a straight line connecting the center of the ONH and the fovea as a reference for separating the hemiretinas. This results, on average, in a 14° and 6° misalignment with the anatomical extended raphe, respectively. For the macular area, the commonly used straight line through the center of the optic disc and the fovea fails to describe the raphe adequately; the disc–fovea–raphe angle is clearly less than 180° (see above). A hallmark of many optic neuropathies, including glaucoma, is a change in retinal thickness that is asymmetrical with respect to the (extended) raphe. Therefore, an accurate localization of the (extended) raphe is pivotal for an optimal assessment of pathology. Because the (extended) raphe appears to coincide almost perfectly with the modified polar coordinate system reference line, no additional measurements or new landmarks are needed for implementing a more accurate location of the (extended) raphe in OCT analysis software. It is sufficient to (1) localize the center of the optic disc and the fovea; (2) assume the optic disc to be located above the equator with (in Cartesian coordinates) a 15:2 (x:y) distance ratio relative to the fovea; (3) assume that the extended raphe has a parabolic shape and the raphe is straight; and (4) require the first derivative of the raphe and extended raphe to be continuous at the fovea. Mathematically speaking, the (extended) raphe is, in Cartesian coordinates for the right eye, given by

$$y(x) = \begin{cases} 2\,(x/15)^2 & x \geq 0 \\ 0 & x < 0 \end{cases} \quad (1)$$

with the fovea at (0,0) and the center of the optic disc at (15,2). Obviously, there are more possible curves that fit to the three involved points (fovea, optic disc center, and evaluated location of the watershed at the OCT reference circle). However, if a straight line between the fovea and optic disc center gives a biased fit at the measurement circle, then a parabola is the simplest next step (parsimony) and also has the elegant property that it connects smoothly (continuity of the first derivative) to the raphe temporal to the fovea.

The translational relevance of our findings is that we have provided a description of the raphe and extended raphe in the retina that is based on anatomy, more accurate than the reference lines used in current clinical OCT devices, and robust against rotation of the eye during image acquisition. The next question is whether or not this description improves the diagnostic performance of OCT. Mwanza et al.[23] compared the diagnostic performance of OCT between an analysis of the pRNFL thickness using a horizontal line through the center of the optic disc as a landmark and an analysis using the fovea–disc angle. They did not observe a significant difference. However, these two landmarks are the blue and red lines in Figure 1; therefore, their findings cannot be used to answer the question of whether or not using the black line as a watershed would improve the diagnostic performance. They focused on the pRNFL only. Another ROI where improvements are to be expected is at the raphe, where the red line in Figure 4 deviates much more from the anatomical watershed. Also, improvements will depend on the analysis methods applied. Taking the mean thickness of a large ROI results in a metric that will not strongly depend on the exact borders but will, on the other hand, overlook subtle, optic nerve disease-specific changes. With the advancement of OCT hardware and analysis algorithms, the importance of smaller ROIs that are more realistically defined will increase. As an example, the

parabolic-shaped extended raphe has been used to delineate the vulnerable macular region (also called macular vulnerability zone) in glaucoma.[19,24] The watershed (raphe and extended raphe) as found in our data by tracing RNFB trajectories appears to correspond to the minimum in RNFL thickness as observed using OCT (figure 4 in Reference 19).

In conclusion, the way in which current OCT brands have implemented the raphe in their analysis software is rather crude and imprecise. The anatomical extended raphe is located more inferiorly in the peripapillary area and the raphe is located more superiorly than currently assumed. An unbiased estimate of the location of the raphe and extended raphe can easily be made using only two already known landmarks (the center of the optic disc and the fovea) and applying a perimetry-inspired assumption regarding the shape of the (extended) raphe. Hence, OCT analysis software that considers the hemifields separately could easily be improved. The effect of this improvement on OCT diagnostic performance has yet to be determined.

Acknowledgments

The authors thank the following colleagues for their contribution to the collection of the two datasets underlying this study: P.J. Airaksinen, W.M. Budde, J.B. Jonas, W.A. Lagreze, L.A. Levin, J. Nevalainen, J. Paetzold, P.A. Sample, J. Schiefer, B. Selig, R. Vonthein, and L.M. Zangwill.

Parts of this manuscript were presented at EVER 2018, European Association for Vision & Eye Research Annual Meeting, Nice, France.

Disclosure: **N.M. Jansonius,** None; **U. Schiefer,** HAAG-STREIT Inc. (C)

References

1. Pierro L, Gagliardi M, Iuliano L, Ambrosi A, Bandello F. Retinal nerve fiber layer thickness reproducibility using seven different OCT instruments. *Invest Ophthalmol Vis Sci*. 2012;53:5912–5920.
2. Springelkamp H, Lee K, Ramdas WD, et al. Optimizing the information yield of 3-D OCT in glaucoma. *Invest Ophthalmol Vis Sci*. 2012;53:8162–8171.
3. Lee K, Sonka M, Kwon YH, Garvin MK, Abramoff MD. Adjustment of the retinal angle in SD-OCT of glaucomatous eyes provides better intervisit reproducibility of peripapillary RNFL thickness. *Invest Ophthalmol Vis Sci*. 2013;54:4808–4812.
4. Jansonius NM, Nevalainen J, Selig B, et al. A mathematical description of nerve fiber bundle trajectories and their variability in the human retina. *Vision Res*. 2009;49:2157–2163.
5. Armaly MF. The size and location of the normal blind spot. *Arch Ophthalmol*. 1969;81:192–201.
6. Rohrschneider K. Determination of the location of the fovea on the fundus. *Invest Ophthalmol Vis Sci*. 2004;45:3257–3258.
7. Wang M, Shen LQ, Boland MV, et al. Impact of natural blind spot location on perimetry. *Sci Rep*. 2017;7:6143.
8. Jansonius NM, Schiefer J, Nevalainen J, Paetzold J, Schiefer U. A mathematical model for describing the retinal nerve fiber bundle trajectories in the human eye: average course, variability, and influence of refraction, optic disc size and optic disc position. *Exp Eye Res*. 2012;105:70–78.
9. Huang G, Gast TJ, Burns SA. In vivo adaptive optics imaging of the temporal raphe and its relationship to the optic disc and fovea in the human retina. *Invest Ophthalmol Vis Sci*. 2014;55:5952–5961.
10. Tanabe F, Matsumoto C, McKendrick AM, Okuyama S, Hashimoto S, Shimomura Y. The interpretation of results of 10-2 visual fields should consider individual variability in the position of the optic disc and temporal raphe. *Br J Ophthalmol*. 2018;102:323–328.
11. Bedggood P, Tanabe F, McKendrick AM, Turpin A. Automatic identification of the temporal retinal nerve fiber raphe from macular cube data. *Biomed Opt Express*. 2016;7:4043–4053.
12. Bedggood P, Nguyen B, Lakkis G, Turpin A, McKendrick AM. Orientation of the temporal nerve fiber raphe in healthy and in glaucomatous eyes. *Invest Ophthalmol Vis Sci*. 2017;58:4211–4217.
13. Bedggood P, Mukherjee S, Nguyen BN, Turpin A, McKendrick AM. Geometry of the retinal nerve fibers from emmetropia through to high myopia at both the temporal raphe and optic nerve. *Invest Ophthalmol Vis Sci*. 2019;60:4896–4903.
14. Chauhan BC, Burgoyne CF. From clinical examination of the optic disc to clinical assessment of the optic nerve head: a paradigm change. *Am J Ophthalmol*. 2013;156:218–227.
15. Choi JA, Kim JS, Park HY, Park H, Park CK. The foveal position relative to the optic disc and the retinal nerve fiber layer thickness profile in myopia. *Invest Ophthalmol Vis Sci*. 2014;55:1419–1426.

16. Denniss J, Turpin A, McKendrick AM. Individualized structure-function mapping for glaucoma: practical constraints on map resolution for clinical and research applications. *Invest Ophthalmol Vis Sci*. 2014;55:1985–1993.
17. Qiu K, Zhang M, Wu Z, et al. Retinal nerve fiber bundle trajectories in Chinese myopic eyes: comparison with a Caucasian based mathematical model. *Exp Eye Res*. 2018;176:103–109.
18. Qiu K, Chen B, Yang J, et al. Effect of optic disc-fovea distance on the normative classifications of macular inner retinal layers as assessed with OCT in healthy subjects. *Br J Ophthalmol*. 2019;103:821–825.
19. Hood DC, Raza AS, de Moraes CG, Liebmann JM, Ritch R. Glaucomatous damage of the macula. *Prog Retin Eye Res*. 2013;32:1–21.
20. Chauvenet W. *A Manual of Spherical and Practical Astronomy*, Vol. 2. 5th ed. Philadelphia, PA: J.B. Lippincott; 1906:469–566.
21. Denniss J, Turpin A, Tanabe F, Matsumoto C, McKendrick AM. Structure-function mapping: variability and conviction in tracing retinal nerve fiber bundles and comparison to a computational model. *Invest Ophthalmol Vis Sci*. 2014;55:728–736.
22. Sugita M, Pircher M, Zotter S, et al. Retinal nerve fiber bundle tracing and analysis in human eye by polarization sensitive OCT. *Biomed Opt Express*. 2015;6:1030–1054.
23. Mwanza JC, Lee G, Budenz DL. Effect of adjusting retinal nerve fiber layer profile to fovea-disc angle axis on the thickness and glaucoma diagnostic performance. *Am J Ophthalmol*. 2016;161:12–21.e1–2.
24. Hood DC, Nguyen M, Ehrlich AC, et al. A test of a model of glaucomatous damage of the macula with high-density perimetry: implications for the locations of visual field test points. *Transl Vis Sci Technol*. 2014;3:5.